

Fishnet metamaterials with incorporated titanium absorption layer

This content has been downloaded from IOPscience. Please scroll down to see the full text.

2013 J. Phys. D: Appl. Phys. 46 495107

(<http://iopscience.iop.org/0022-3727/46/49/495107>)

View [the table of contents for this issue](#), or go to the [journal homepage](#) for more

Download details:

This content was downloaded by: evgeny_mironov

IP Address: 131.236.55.156

This content was downloaded on 23/02/2014 at 02:20

Please note that [terms and conditions apply](#).

Fishnet metamaterials with incorporated titanium absorption layer

E G Mironov¹, W J Toe², P J Reece² and H T Hattori¹

¹ School of Engineering and Information Technology, The University of New South Wales, Canberra ACT 2610, Australia

² School of Physics, The University of New South Wales, Sydney, NSW 2052, Australia

E-mail: evgeny.mironov@student.adfa.edu.au

Received 12 August 2013, in final form 23 September 2013

Published 15 November 2013

Online at stacks.iop.org/JPhysD/46/495107

Abstract

Some metamaterial applications require the use of high-power lasers, but the incoming radiation may damage the metamaterials. In addition to that, the presence of an absorptive material placed close to metamaterial surface can lead to quick heating of the surrounding area, resulting in serious thermal damage or melting of the fabricated pattern. We study the impact of a titanium absorptive layer on top of a conventional fishnet structure and we show that due to increased absorption the melting power is reduced by nearly 50% and thermal damage leads to the formation of microbumps on the exposed surface.

(Some figures may appear in colour only in the online journal)

1. Introduction

Metamaterials are artificial micro- and nano-structures that allow the control of light propagation in a certain medium. Since the dimensions of metamaterials are significantly smaller than the wavelength of light, the incoming radiation does not distinguish individual cells, but treats the array as a homogeneous medium. The most important feature of a metamaterial is that its geometry uniquely determines the effective refractive index of the medium and, as such, it is possible to tailor a metamaterial's macroscopic electromagnetic response to bend light in any prescribed direction. Most of the metamaterial research is focused on creating negative refractive index materials (NIMs) and producing effects such as super resolution [1], optical magnetism [2] and cloaking [3].

Recently, much attention has been drawn to nonlinear effects in NIM metamaterial such as second and third harmonic generation [4], four-wave mixing [5] and parametric amplification [6]. The excitation of these effects generally requires high powers, which leads to high fluence (energy per unit area). However, this can potentially result in thermal damage of the structure when the incoming radiation is absorbed by metal and energy is transferred to the lattice due to electron–phonon coupling [7].

Many optical metamaterials use gold as its metal component because of its relatively low losses in the optical frequency region. Whilst gold has a melting point of only 1064 °C under normal conditions, it is highly reflective and

only absorbs a small fraction of incoming radiation ($\sim 3\%$). On the other hand, materials such as titanium, which is commonly used in plasmonic devices for adhesion purposes [8, 9], have higher absorption that can result in a quick temperature rise of the surrounding media. While titanium has a higher melting point of 1660 °C under normal conditions and remains mostly unaffected during exposure, it can induce deformation in the adjacent gold layer because of the elasto-plastic flow that results in microbumps and nanojets formations [10].

In this article we study the behaviour of the fishnet metamaterial fabricated with different fractions of titanium absorption layer. While keeping the total height of the fishnet constant, we decrease the thickness of the top gold layer by replacing it with titanium, which increases absorption. These metamaterials are designed to have a negative refractive index around 281 THz and we irradiate them with a 1064 nm continuous wave Nd : YAG laser in order to find the structure's power damage threshold. We show that due to increased absorption, the titanium layer significantly reduces the structure melting threshold compared to the case of pure gold fishnet metamaterial. We also demonstrate that thermal effects result in the formation of microbumps on the fishnet surface.

2. Theoretical analysis of device

The fishnet structure consists of alternating metal–dielectric layers with periodical rectangular holes and is placed on top of the quartz substrate, as shown in figure 1. Each material

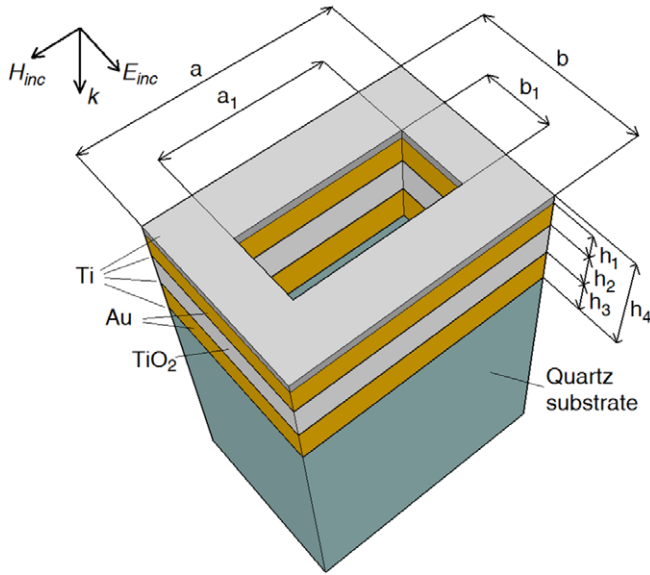


Figure 1. Metamaterial cell.

layer is separated by a 2 nm thick adhesion titanium layer. The geometry is studied by using numerical commercial software CST Microwave Studio 2012 to produce a negative refractive index at 1064 nm and is simulated by using a frequency domain solver. Metals are modelled as dispersive materials with multiple resonant frequencies according to a multi-resonance Lorentzian model [11, 12]. Due to measurement setup design, the sample should be placed in water during the experiment, thus the superstratum is modelled with a refractive index $n_{\text{water}} = 1.325$. The Floquet ports along the k -vector direction (input and output) are terminated by perfectly absorbing layers [13]. The wave is normally incident on the structure, as shown in figure 1, and the incident mode is assumed to be TE (with the main electric field component as shown in figure 1). The dielectric media, titanium dioxide (TiO_2) and quartz have refractive indices of 2.7 and 1.53, respectively. The transmission and reflectance spectra are calculated from obtained S-parameters as $T = |S_{21}|^2$ and $R = |S_{11}|^2$. Effective refractive index n_{eff} is then extracted using the standard approach [14]:

$$n_{\text{eff}} = \pm \frac{1}{kh} \cos^{-1} \left(\frac{1}{T} \frac{n_1(1 - R^2) + n_3 T^2}{n_1 + n_3 + R(n_3 - n_1)} \right), \quad (1)$$

where k is a wave vector in vacuum, h is the total height of fishnet, n_1 is the refractive index of the superstratum (water) and n_3 is the refractive index of the substrate (quartz). The sign is chosen in such a way that the imaginary part of n_{eff} will always remain positive since the material is considered to be lossy and the wave can only decay while propagating. The plots for real and imaginary parts of n_{eff} as a function of frequency are shown in figure 2. The variation of gold and titanium thickness ratio in upper layer is described with filling factor G that varies from 0 to 1:

$$G = \frac{h_{\text{Ti}}}{h_{\text{Ti}} + h_{\text{Au}}}, \quad (2)$$

where h_{Ti} is the thickness of titanium absorption layer and h_{Au} is the thickness of remaining gold in the top layer of fishnet. Only the top layer has titanium on it, whilst other metallic layers are made of gold only. Note that the total thickness of the top metallic layer is kept constant at 50 nm. Also, neither the thicknesses of the bottom Au layer, nor the dielectric TiO_2 layer, are changed. Different filling factors in figure 2 are represented in the following way: \circ ($G = 0$, only gold in the top layer), \square ($G = 0.35$), \bullet ($G = 0.5$), \times ($G = 0.7$), $+$ ($G = 1$, only titanium in the top layer). The points for real part of refractive index are connected with a continuous line. As is expected, due to higher plasmonic losses the resonance gap becomes shallower with increase of titanium fraction and then eventually disappears. The values of the effective refractive indices for $G = 0$ and $G = 0.35$ are -0.6125 and -0.0854 , respectively. As can be observed in figure 2 for $G = 0.5$, $G = 0.7$ and $G = 1$, n_{eff} is positive for all wavelengths in the considered region of interest. The simulations show that the effective refractive index becomes positive for $G > 0.42$. Thus, investigations for $G = 0.7$ and $G = 1$ are used only to illustrate the impact of higher content of titanium on absorption, although the refractive index is not negative.

The fishnet structure is designed to operate at 1064 nm: simultaneously creating negative index material and having titanium as an upper absorption layer. The dimensions of the metamaterial cell are summarized in table 1.

We have fabricated structures with different filling factors: $G = 0$ (50 nm of Au), $G = 0.35$ (32.5 nm of Au, 17.5 nm of Ti), $G = 0.7$ (15 nm of Au, 35 nm of Ti) and $G = 1$ (50 nm of Ti). Since only transmission T , reflection R and absorption A are considered in the numerical simulations, the latter parameter can be calculated as $A = 1 - T - R$. The frequency response of absorption and reflection for the selected filling factors are shown in figures 3(a) and (b). Resonance behaviour of refractive index results in the rise of absorption (figure 3(a)) as well as in the drop of reflectivity (figure 3(b)). For pure gold ($G = 0$) the absorption mainly occurs because of NIM resonance, while metamaterial with the incorporated titanium layer has a weak electromagnetic resonance, and higher absorption is achieved because of titanium itself ($G = 1$). The combination of metamaterial resonance and material losses introduced by a titanium layer results in even higher absorption ($G = 0.35$, $G = 0.7$), presented in figure 3(a). It is also noted that due to differences in plasma frequencies between titanium and gold the absorption resonance red-shifts and smoothens with increasing filling factor. As an additional reference, we plot absorption and reflection spectra for a metal–dielectric layered structure that lacks a hole (figures 4(a) and (b), respectively). The absorption around 1064 nm gradually increases with higher filling factors reaching almost 52%.

In table 2 the calculated values of reflection, transmission and absorption (at 1064 nm) are presented for fabricated fishnet structures with different filling factors and layered metal–dielectric structures (with no air holes, only plain structures with different layers). For the fishnet structure, the addition of titanium effectively increases the global absorption of the structure, but weakens the resonance. For non-patterned

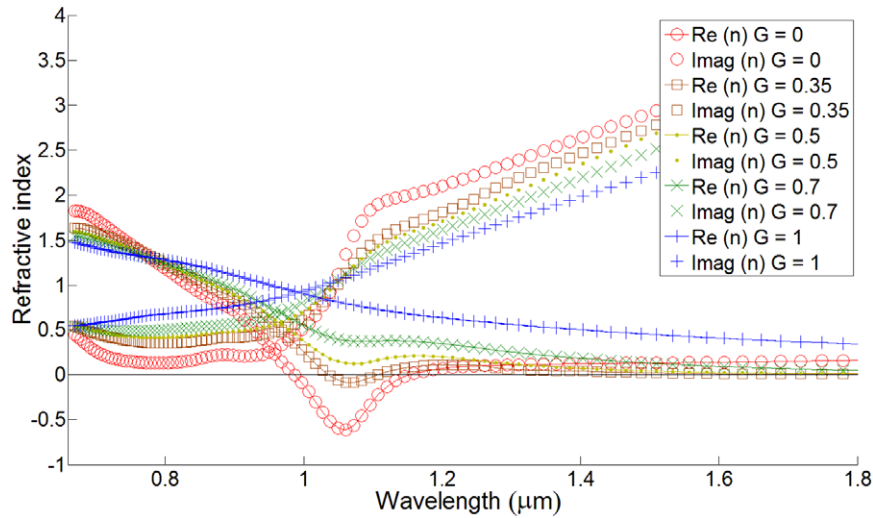


Figure 2. Extracted refractive index.

Table 1. Geometrical dimensions of the metamaterial cell.

| Variable | Description | Value (nm) |
|----------|-------------------------------------|------------|
| a | Length of cell | 350 |
| b | Width of cell | 240 |
| a_1 | Length of gap | 225 |
| b_1 | Width of gap | 113 |
| h_1 | Thickness of upper Au layer | 0–50 |
| h_2 | Thickness of TiO ₂ layer | 50 |
| h_3 | Thickness of lower Au layer | 50 |
| h_4 | Total thickness | 156 |

multi-layered structure, gold, as expected, acts as a good mirror, while titanium partially absorbs the incident radiation.

In general, the damage of a material is associated with the absorbed fluence F of an incident light field [7]. For a continuous wave laser with spot-size d , exposure time T , incident power P and absorption A , the fluence is approximately:

$$F = \frac{4TPA}{\pi d^2}. \quad (3)$$

Because of the limitations in our experimental setup, we limit ourselves to exposing the samples to a fixed time of 2 min. Real-time thermal damage assessment is not possible due to constrained capabilities of our imaging system.

The underlying physics of material deformation resulting from laser–metal interaction could be explained with a combination of elasto-plastic flow and two-temperature model (TTM) in a two-dimensional approximation [10]. Elasto-plastic flow depicts the mechanical lattice deformation of the exposed surface, while TTM [10, 15–18] describes the melting of metal due to absorption of incoming radiation by electrons with subsequent electron–phonon coupling. The equations for dynamic elasticity can be found in [19]. Then the plastic yielding could be estimated by taking into account the von-Mises yield criterion in terms of the stress deviator [10, 20].

Schematically, the deformation process is visualized in figures 5(a)–(c). During exposure, laser radiation impinges

at normal incidence to the studied sample (figure 5(a)). As a result of electron–phonon coupling the metallic layer exhibits momentum normal to the surface. While at least some part of the layer remains solid, this momentum is compensated by the work of plastic deformations leading to the formation of a microbump or nanojet on top of the sample (figures 5(b) and (c)). Eventually, with increase of fluence, the metallic layer momentum exceeds surface tension forces (for liquid phase), as well as the work of plastic deformations (for solid phase) and nanojet bursts. Microbump with clear nanojet formation could be seen in figure 5(d). It was obtained with maximum incident laser power of 140 mW on top of our metal–dielectric structures.

Several factors influence the formation of microbumps such as melting temperature, Young’s modulus and coefficient of linear thermal expansion [21]. The low values of these parameters correspond to small potential mechanical energy, consequently smaller amounts of laser radiation are required to overcome the work of plastic deformations [10]. On the other hand, material plasticity should remain high to prevent premature bursts. Based on the material properties given in [22] titanium can potentially form microbumps during irradiation, and gold nanojets have been already experimentally demonstrated in [21, 23].

3. Experimental results

All samples are fabricated on top of a quartz substrate. Metallic parts are deposited by using the electron beam evaporator system and a dielectric layer is deposited by using a sputter system. The thicknesses of materials are given in table 1 and filling factors are $G = 0$, $G = 0.35$, $G = 0.7$ and $G = 1$. The fishnet holes are milled by using FEI Helios NanoLab 600 dual-beam FIB system at a low current of 9.7 pA to prevent any undesirable damage to the structure. On each sample we have patterned 3 fishnet arrays with areas of 225 μm^2 (figure 6). Patterns are placed 100 μm away from each other allowing exposing them individually. Every metamaterial array consists

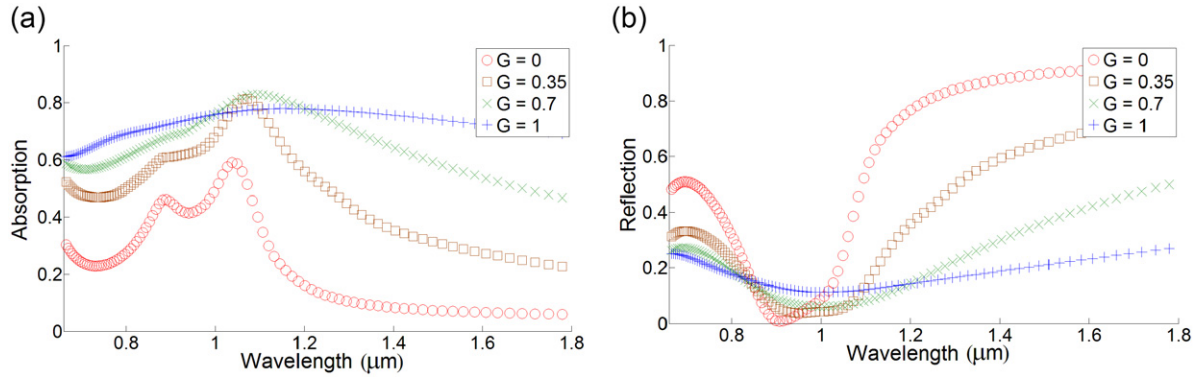


Figure 3. (a) Absorption spectrum for fishnet structure. (b) Reflection spectrum for fishnet structure.

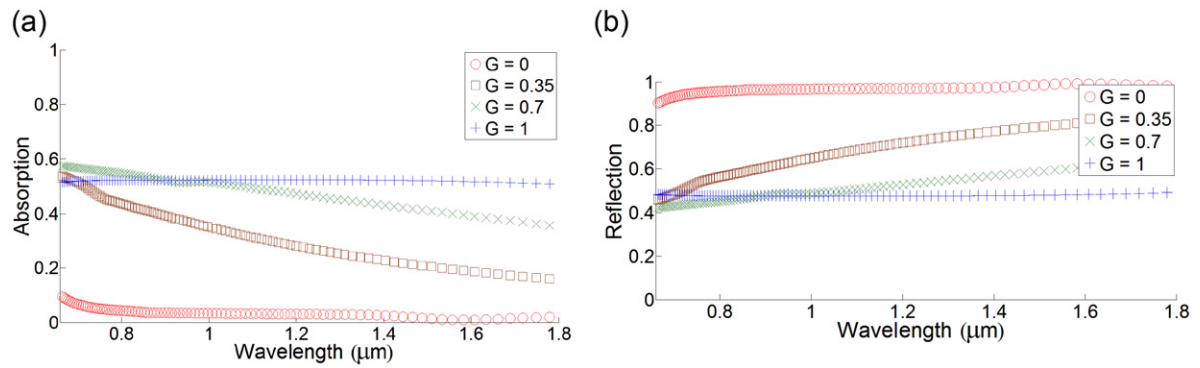


Figure 4. (a) Absorption spectrum for layered metal–dielectric structure. (b) Reflection spectrum for layered metal–dielectric structure.

Table 2. Simulated values of reflection, transmission and absorption at 1064 nm.

| Filling factor | Fishnet structure | | | Layered metal–dielectric structure | | |
|----------------|-------------------|--------------|------------|------------------------------------|--------------|------------|
| | Reflection | Transmission | Absorption | Reflection | Transmission | Absorption |
| 0 | 0.3345 | 0.1186 | 0.5469 | 0.9682 | 0 | 0.0318 |
| 0.35 | 0.0700 | 0.1166 | 0.8134 | 0.6738 | 0 | 0.3262 |
| 0.7 | 0.0689 | 0.1109 | 0.8202 | 0.4987 | 0 | 0.5013 |
| 1 | 0.1167 | 0.1114 | 0.7719 | 0.4775 | 0 | 0.5225 |

of 3920 elements, preventing any local inhomogeneities or fabrication flaws to affect the total performance of the structure.

A draft of the experimental setup is shown in figure 7. The 1064 nm CW Nd:YAG (Laser Quantum, IR Ventus) laser is focused down to a diffraction limited spot using a microscope objective lens (Nikon CFI Plan Achromat 100×). This is achieved by expanding the laser to slightly over-fill the back aperture of the objective lens. A spatial light modulator (SLM) (Hamamatsu, LCOS) is also preconfigured to minimize aberrations at the laser focus. With these arrangements, a spot size of 0.8 μm is achieved at the laser focus (it is assumed that the laser has Gaussian profile and spot diameter is defined by containing 95% of the total beam power). The laser power at the focus is controlled by using a polarizing beam splitter together with a half wave plate. Taking all optical losses into account, a maximum incident power of 140 mW is achievable at the laser focus.

The substrates with nanostructure arrays are mounted on top of a glass slide and covered with type-0 cover slips, with a thin film of water (20 μm) in between for refractive index

matching. A CCD camera is used to image the surface of the substrate and locate the nanostructure arrays. Once located, the nanostructure arrays are illuminated at a fixed laser power for 2 min. As an additional reference, we also expose an unpatterned area away from the metamaterial array using the same illumination conditions. In subsequent experiments laser power is gradually increased in a step of 15 mW. After each exposure the laser spot is moved to a new position of the patterned area to ensure that damage will not accumulate in one point. Between experiments, the structures are first visually inspected via the CCD camera for the macroscopic signs of microbump and nanojet formations.

Experiments show a good agreement with our expectations: SEM images of exposed surface demonstrate significant thermal damage that is proportional to the illumination power. The formation process of a microbump is clearly observed in figures 8–10. When the laser power exceeds threshold value, the underlying gold layer starts melting and deforming titanium film above (figure 8). As the power is increased from 60 to 90 mW the affected area grows

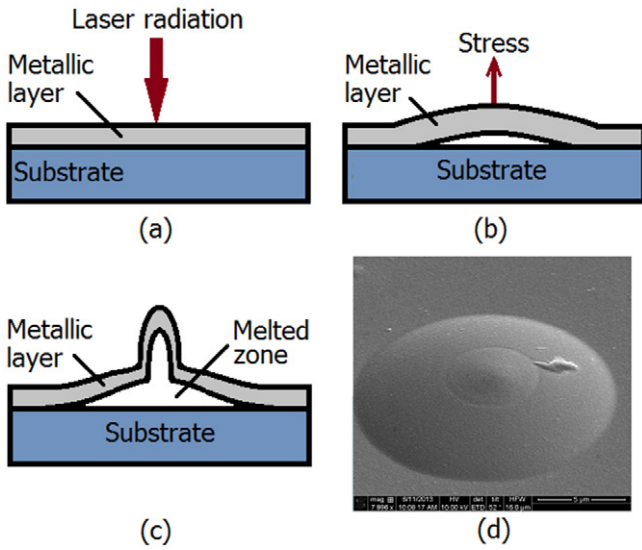


Figure 5. (a) The deformation of metallic layer during exposure. (b) Formation of microbump and (c) nanojet. (d) SEM image of the experimentally obtained structure.

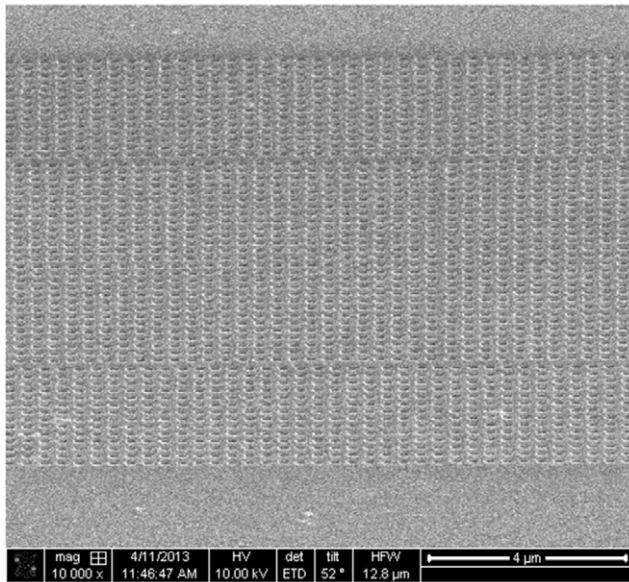


Figure 6. Fabricated fishnet.

by nearly 6 times (figure 9). The exposure with maximum laser power of 140 mW results in a formation of microbump with a diameter of 1.5 μm (figure 10). The microbump burst is presented in figure 11. During the irradiation the underlying gold layer forms an unstable microbump and eventually blows the titanium film above, warping both materials and leaving the traces of melted metals around the exposed spot. The high magnification SEM images of exposed surface also show the rectangular holes tend to form more rounded shapes close to the melting regions. This can be attributed to surface tension effects.

In the experiments, we have studied the dependence of damaging laser power on the Au/Ti ratio in the top layer (i.e. on sample absorption). The thermal damage of metamaterials occurred at the following incident powers: $P_0 = 88$ mW, $P_{0.35} = 53$ mW, $P_{0.7} = 45$ mW, $P_1 = 60$ mW where index

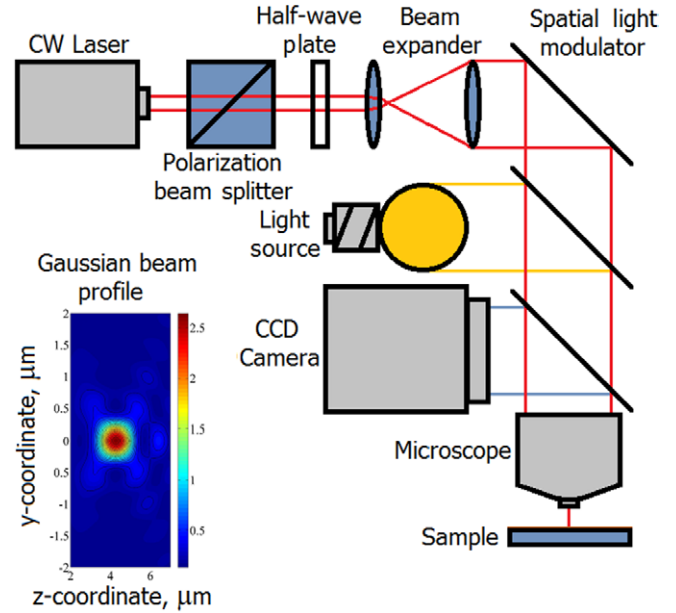


Figure 7. Experimental setup.

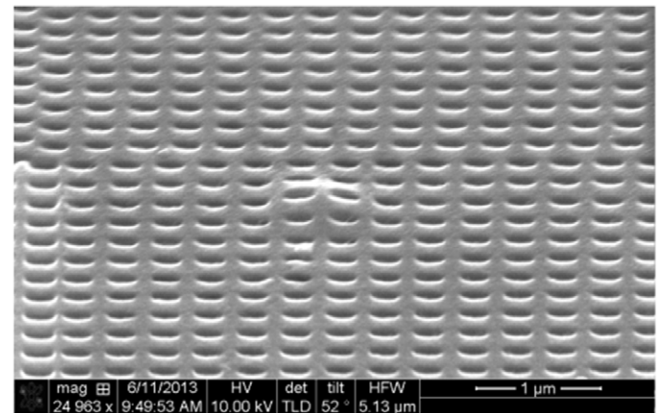


Figure 8. Microbump formation, power 60 mW, $G = 0.35$.

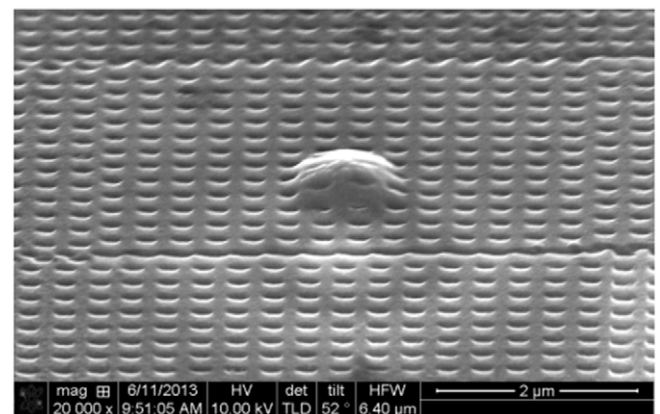


Figure 9. Microbump formation, power 90 mW, $G = 0.35$.

correspond to the filling factor G . Then the absorbed damaging power is calculated as multiplication of absorption on incident damaging power, given in mW. The calculated results are summarized in table 3.

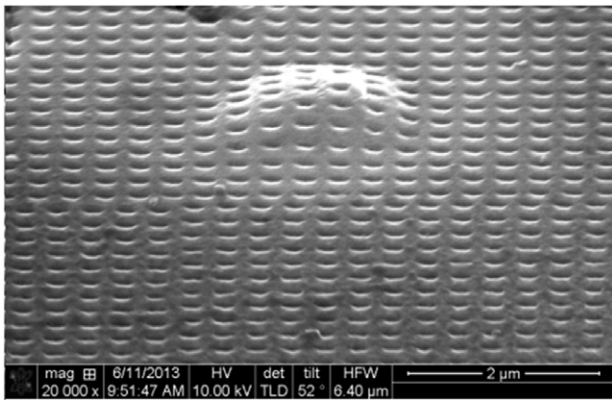


Figure 10. Microbump formation, power 140 mW, $G = 0.35$.

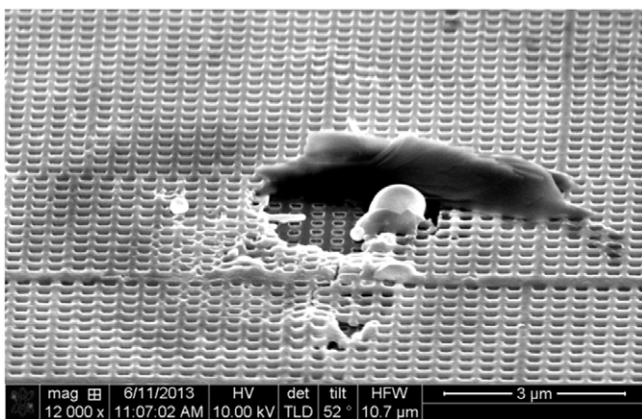


Figure 11. Microbump burst, power 140 mW, $G = 0.7$.

Table 3. Summarized results.

| Filling factor | Calculated Reflection | Calculated Transmission | Calculated Absorption | Incident damaging power (mW) | Absorbed damaging power (mW) |
|----------------|-----------------------|-------------------------|-----------------------|------------------------------|------------------------------|
| 0 | 0.3345 | 0.1186 | 0.5469 | 88 | 48.1272 |
| 0.35 | 0.0700 | 0.1166 | 0.8134 | 53 | 43.1102 |
| 0.7 | 0.0689 | 0.1109 | 0.8202 | 45 | 36.9090 |
| 1 | 0.1167 | 0.1114 | 0.7719 | 60 | 46.3140 |

For reference, we also exposed unpatterned areas and observed the formation of microbumps, as presented in figure 5(d). Due to smaller absorption of the metallic layers, the incident power was increased above 90 mW, but in this region the laser does not operate stably and it is very hard to find the exact damaging thresholds. However, the melting order of the samples remained correct and samples with higher fraction of gold required significantly more power. With a maximum possible incident power of 140 mW all samples were eventually melted. We could say that the absorbed damaging power for titanium was above 70 mW whilst the absorbed damaging power for gold was above 4 mW.

4. Conclusion

In this article, we analysed the impact of a titanium layer on the absorption of a conventional fishnet structure. Our

metamaterials were exposed to 1064 nm CW Nd : YAG laser for 2 min each and then the thermal damage was assessed from SEM images. We showed that combination of titanium and gold increased the total absorption of metamaterials to nearly 82% and led to the decrease of damage threshold power to 45 mW (51% of original incident damaging power and 77% of original absorbed damage threshold power). We also found that the melting process resulted in the formation of microbumps in the top fishnet layer: these microbumps are the result of the melting of the gold underlayer, which leads to a mechanical deformation of the solid titanium film. The possible applications of such metamaterials with enhanced absorption are sensors or thermal fuses in optical circuits. While being transparent around resonance frequency at low powers they melt and block the light path after laser radiation exceeds a certain threshold.

Acknowledgments

This work was supported by the Australian National Fabrication Facility (ANFF) and the Australian Research Council (ARC) Grant Number DP 110100713.

References

- [1] Casse B D F *et al* 2010 Super-resolution imaging using a three-dimensional metamaterials nanolens *Appl. Phys. Lett.* **96** 023114
- [2] Urzhumov Y A and Shvets G 2008 Optical magnetism and negative refraction in plasmonic metamaterials *Elsevier Solid State Commun.* **146** 208–20
- [3] Cai W *et al* 2007 Optical cloaking with metamaterials *Nature Photon.* **1** 224–7
- [4] Shadrivov I V *et al* 2006 Second-harmonic generation in nonlinear lefthanded metamaterials *J. Opt. Soc. Am. B* **23** 529–34
- [5] Popov A K *et al* 2007 Four-wave mixing, quantum control, and compensating losses in doped negative-index photonic metamaterials *Opt. Lett.* **32** 3044–6
- [6] Popov A K and Shalaev V M 2006 Compensating losses in negative-index metamaterials by optical parametric amplification *Opt. Lett.* **31** 2169–71
- [7] Sobral H and Villagrán-Muniz M 2005 Energy balance in laser ablation of metal targets *J. Appl. Phys.* **98** 083305
- [8] Aksu S *et al* 2010 High-throughput nanofabrication of infrared plasmonic nanoantenna arrays for vibrational nanospectroscopy *Nano Lett.* **10** 2511–8
- [9] Lahiri B *et al* 2010 Impact of titanium adhesion layers on the response of metallic split-ring resonators (SRRs) *Opt. Express* **18** 11202–8
- [10] Meshcheryakov Y P and Bulgakova N M 2006 Thermoelastic modeling of microbump and nanojet formation on nanosize gold films under femtosecond laser irradiation *Appl. Phys. A* **82** 363–8
- [11] 1999 Fullwave 6.0 RSOFT Design Group, www.rsoftdesign.com
- [12] Hattori H T *et al* 2009 Coupling of light from microdisk lasers into plasmonic nano-antennas *Opt. Express* **17** 20878–84
- [13] Hattori H T 2008 Analysis of optically pumped equilateral triangular microlasers with three mode-selective trenches *Appl. Opt.* **47** 2178–85
- [14] Menzel C *et al* 2008 Retrieving effective parameters for metamaterials at oblique incidence *Phys. Rev. B* **77** 195328

- [15] Kaganov M I *et al* 1957 Relaxation between electrons and crystalline lattices *Sov. Phys.—JETP* **4** 173
- [16] Anisimov S I *et al* 1974 Electron emission from metal surfaces exposed to ultrashort laser pulses *Sov. Phys.—JETP* **39** 375
- [17] Wellershoff S-S *et al* 1999 The role of electron–phonon coupling in femtosecond laser damage of metals *Appl. Phys. A* **69** S99–107
- [18] Bulgakova N M and Bourakov I M 2002 Phase explosion under ultrashort pulsed laser ablation: modeling with analysis of metastable state of melt *Elsevier Appl. Surf. Sci.* **197** 41–44
- [19] Timoshenko S P 1972 *Course of Theory of Elasticity* (Kiev: Naukova Dumka) (in Russian)
- [20] Wilkins M L 1964 Calculation of elastic–plastic flow *Methods in Computational Physics (Fundamental Methods in Hydrodynamics* vol 3) (New York: Academic)
- [21] Korte F *et al* 2004 Formation of microbumps and nanojets on gold targets by femtosecond laser pulses *Appl. Phys. A* **79** 879
- [22] Bobylev A V 1987 *Mechanical and Technological Properties of Metals* (Moscow: Metallurgia) (in Russian)
- [23] Koch J *et al* 2005 Nanotexturing of gold films by femtosecond laser-induced melt dynamics *Appl. Phys. A* **81** 325